Fe/Co Alloys for the Catalytic Chemical Vapor Deposition Synthesis of Single- and Double-Walled Carbon Nanotubes (CNTs). 2. The CNT−Fe/Co−$MgAl_2O_4$ System

Pierre Coquay,[†] Emmanuel Flahaut,[‡] Eddy De Grave,[†] Alain Peigney,[‡] Robert E. Vandenberghe,[†] and Christophe Laurent*[,‡]

NUMAT, Department of Subatomic and Radiation Physics, University of Ghent, Proeftuinstraat 86, B-9000 Gent, Belgium, and CIRIMAT UMR CNRS-UPS-INP 5085, Centre Interuniversitaire de Recherche et d'Ingénierie des Matériaux, Université Paul-Sabatier, 31062 Toulouse Cedex 9, France

Received: May 12, 2005; In Final Form: July 20, 2005

A detailed ^{57}Fe Mössbauer study of the $Mg_{0.8}Fe_{0.2-y}Co_yAl_2O_4$ ($y = 0$, 0.05, 0.1, 0.15, 0.2) solid solutions and of the CNT−Fe/Co−$MgAl_2O_4$ nanocomposite powders prepared by reduction in H_2−CH_4 has allowed characterization of the different iron phases involved in the catalytic process of carbon nanotube (CNT) formation and to correlate these results with the carbon and CNT contents. The oxide precursors consist of defective spinels of general formulas $(Mg_{1-x-y}^{2+}Fe_{x-3\alpha}^{2+}Fe_{2\alpha}^{3+}\square_\alpha Co_y^{2+}Al_2^{3+})O_4^{2-}$. The metallic phase in the CNT−Fe/Co−$MgAl_2O_4$ nanocomposite powders is mostly in the form of the ferromagnetic α-Fe/Co alloy with the desired composition. For high iron initial proportions, the additional formation of Fe_3C and γ-Fe−C is observed while for high cobalt initial proportions, the additional formation of a γ-Fe/Co−C phase is favored. The higher yield of CNTs is observed for postreaction α-$Fe_{0.50}Co_{0.50}$ catalytic particles, which form no carbide and have a narrow size distribution. Alloying is beneficial for this system with respect to the formation of CNTs.

Introduction

Catalytic chemical vapor deposition (CCVD) methods have a great potential for low-cost, large-scale production synthesis of carbon nanotubes (CNTs) and furthermore offer the possibility to form the CNTs either inside a host material or very locally on patterned substrates. These methods, basically similar to those used for several decades for the synthesis of filamentous carbon, involve the catalytic decomposition of a carbonaceous gas (hydrocarbon or carbon monoxide) on transition-metal nanometric particles. Although several mechanisms do exist, CNTs with only one or two walls (SWNTs and DWNT, respectively) are mainly produced by catalyst particles below ca. 3 nm in diameter.[1−4] Iron and cobalt have both found to be effective for the production of SWNTs and DWNTs, but interestingly several authors[5−8] have reported that Fe/Co alloys, sometimes referred to as bimetallic catalysts, are even more effective. The alloy formation or composition was not studied precisely, but the $Fe_{0.50}Co_{0.50}$ composition was nevertheless sometimes singled out as a particularly interesting one.[5,6,8] By contrast, the Fe/Co alloys involved in the formation of multiwalled CNTs (MWNTs).[9−16] were often studied in greater detail, notably by Mössbauer spectroscopy[11−15] and X-ray photoelectron spectroscopy.[16] Note that the size of these Fe/Co particles is much higher, in the range 20−40 nm, and that the formation mechanisms of the MWNTs are different from those of the SWNTs and DWNTs. It was notably reported[11,12] that the most efficient alloy, in terms of stability toward oxidation and carburization reactions, has a composition close to $Fe_{0.50}Co_{0.50}$ and that avoiding the formation of Fe_3C was indeed beneficial for the formation of MWNTs. The latter point was also reported in the case of SWNTs and DWNTs.[4,5,17]

The present authors have proposed an original CCVD method[18] where pristine metal nanoparticles are formed in situ at a temperature high enough for them to catalyze the decomposition of CH_4 and the subsequent formation of CNTs. In this method, an oxide starting material is reduced in a H_2−CH_4 atmosphere to produce a CNT−metal−oxide powder. A study[19] on CNT−M−$MgAl_2O_4$ (M = Fe, Co, Ni) nanocomposite powders revealed that for all the studied transition metal contents, the highest CNT quantities were given by cobalt, then iron, and then nickel and the best carbon qualities (notably reflecting a minimum of fiberlike species) are given by cobalt, then nickel, and then iron. It was further shown[5] that alloying provides intermediate results in the case of Fe/Ni and Co/Ni but that, interestingly, Fe/Co alloys were found to produce more CNTs than either Fe or Co although the carbon quality was slightly inferior to that obtained for pure cobalt. The differences between iron and cobalt could find their origin both in the formation of cementite (Fe_3C) particles and in a higher particle size in the case of iron. Indeed, studies of the carbon-free nanocompsoite powders[20,21] revealed that the metal particle size distribution is bimodal (<30 nm and 50−200 nm) for Fe−$MgAl_2O_4$ but unimodal and rather narrow for Fe/Co- and Co−$MgAl_2O_4$ (10−15 nm). ^{57}Fe Mössbauer spectroscopy investigation of the CNT−Fe−$MgAl_2O_4$[17,22,23] powders have revealed three iron phases (ferromagnetic α-Fe, ferromagnetic Fe_3C, and a γ-Fe−C alloy showing antiferromagnetic coupling below 80 K). The study suggests that (i) the particles that catalyze the formation of the CNTs are Fe_3C in postreaction examination, (ii) the particles located inside the spinel grains are α-Fe particles

* To whom correspondence should be addressed. Tel: +33 (0)5 61 55 61 22. Fax: +33 (0)5 61 55 61 63. E-mail: laurent@chimie.ups-tlse.fr.

[†] NUMAT, Department of Subatomic and Radiation Physics, University of Ghent.

[‡] CIRIMAT UMR CNRS-UPS-INP 5085, Centre Interuniversitaire de Recherche et d'Ingénierie des Matériaux, Université Paul-Sabatier.

10.1021/jp052494y CCC: $30.25
Published on Web 09/02/2005

and small γ-Fe−C particles, and (iii) the inactive carbon-coated particles could end up as any of the α-Fe, Fe_3C, and γ-Fe−C forms.

In this context, we have performed a detailed ^{57}Fe Mössbauer spectroscopy investigation of the Fe/Co alloys involved in the formation of SWNTs and DWNTs for the CNT-Fe/Co−$MgAl_2O_4$ system. Characterization of the same materials by X-ray diffraction (XRD), electron microscopy and by a macroscopical method based on specific-surface-area measurements[18,24] were reported elsewhere.[5] In particular, XRD pattern have shown that the involved oxide solid solutions are pure, single-phase spinel phases. This work also builds on several papers dealing with Co−$MgAl_2O_4$,[20] Fe−$MgAl_2O_4$,[22] Fe/Co−$MgAl_2O_4$,[21] CNT−M−$MgAl_2O_4$ (M = Fe, Co, Ni),[19] and CNT−Fe−$MgAl_2O_4$[17,22,23] composite powders, as well as the relevant (Mg, Fe, Co)Al_2O_4 oxides used as starting materials. Results for the CNT−Fe/Co−MgO system will be reported in a companion paper.[25]

Experimental Section

Synthesis. Spinel oxides were prepared by the nitrate−urea combustion route[26] as described elsewhere.[5,19] Six grams of oxide solid solution powders with the desired formula $Mg_{0.8}Fe_{0.2}Al_2O_4$, $Mg_{0.8}Fe_{0.15}Co_{0.05}Al_2O_4$, $Mg_{0.8}Fe_{0.1}Co_{0.1}Al_2O_4$, $Mg_{0.8}Fe_{0.05}Co_{0.15}Al_2O_4$ and $Mg_{0.8}Co_{0.2}Al_2O_4$ were produced. For the sake of brevity, the oxide powders will be referred to in the following as Fe20, Fe15Co5, Fe10Co10, Fe5Co15, and Co20. The CNT−Fe/Co−$MgAl_2O_4$ nanocomposite powders were obtained[5,19] by selective reduction in a H_2-CH_4 atmosphere (18 mol % CH_4) of the oxide powders prepared by combustion. The reaction was carried out at atmospheric pressure in a fixed-bed flow reactor. The thermal cycle was the following: heating rate of 5 °C/min up to 1070 °C, 6 min dwell at 1070 °C, cooling rate of 5 °C/min to room temperature (RT). For the sake of brevity, the CNT−Fe/Co−$MgAl_2O_4$ nanocomposite powders will be referred to in the following as Fe20R, Fe15Co5R, Fe10Co10R, Fe5Co15R and Co20R, respectively, where "R" stands for "reduced".

Characterization. Mössbauer spectra (MS) of the iron-containing specimens were recorded with a ^{57}Co (Rh) source using a conventional time-mode spectrometer with a constant-acceleration drive and a triangular-reference signal. Accumulation of the data was performed in 1024 channels until a background of at least 10^6 counts per channel was reached. The spectrometer was calibrated by collecting at RT the MS of a standard α-Fe foil and the isomer-shift values quoted hereafter are with reference to this standard. Unless otherwise stated, the spectra of the nanocomposite powders were analyzed assuming symmetrical components with a Lorentzian line shape, while those of the oxide powders were fitted with a superposition of a ferrous and a ferric quadrupole-splitting distribution (QSD) with Lorentzian-shaped elemental doublets. For most samples, spectra were recorded at 80 K and at RT to detect a possible evolution of the Fe phases. In addition, selected specimens were examined at different temperatures between 11 K and RT.

Results and Discussion

Mössbauer Spectroscopy Study of the Oxide Powders. A typical MS of the iron-containing oxide powders recorded at 80 K is shown in Figure 1. The relevant parameters obtained from the two QSD fits are listed in Table 1. For specimens with an iron content below 20 atom %, a slightly better fit of the MS is obtained by adding a linear correlation between the isomer shift and the quadrupole splitting for both QSDs, as previously observed for similar oxides.[21] The Fe^{2+} QSD profiles obviously are consistently composed of two more or less distinct components, centered around ∼2.1 and ∼2.9 mm/s, respectively (Figure 1b). Since the spinel lattice has octahedral and tetrahedral lattice sites, it is tempting to ascribe the two components to Fe^{2+} cations being distributed among these two coordination types. Unlike the cobalt-free $Mg_{1-x}Fe_xAl_2O_4$ powders, for which the calculated Fe^{3+} QSD profiles are clearly bimodal,[17] the present $Mg_{0.8}(Fe/Co)_{0.2}Al_2O_4$ samples do not exhibit this feature. The shallow bump in the $p(\Delta E_Q)$ curve observed for $\Delta E_Q \approx$ 1.8 mm/s (see Figure 1c) is insignificant and can be attributed to an artifact of the fitting procedure. In view of the preceding, this would imply that the ferric cations prefer only one type of coordination. According to the isomer-shift data presented in Table 1, this would likely be the octahedral site. More specific details about the Fe cation distribution in the respective spinel phases cannot be concluded from the present MS.

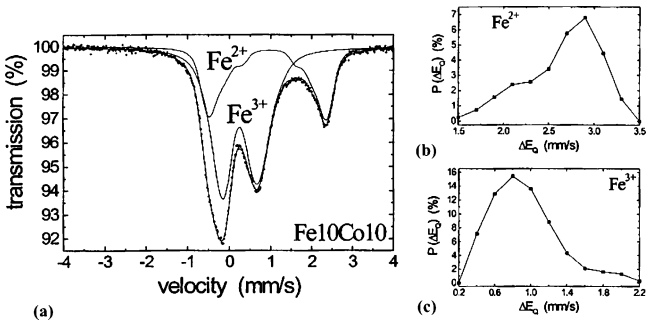

Figure 1. MS of Fe10Co10 (a) measured at 80 K and corresponding quadrupole-splitting distributions of the Fe^{2+} (b) and Fe^{3+} (c) doublets.

TABLE 1: Mössbauer Parameters of the Fe20, Fe15Co5, Fe10Co10, and Fe5Co15 Oxide Powders Measured at 80 K[a]

oxide powder		para Fe^{2+}				para Fe^{3+}			
		δ	ΔE_Q	Γ	P	δ	ΔE_Q	Γ	P
Fe20	(1)	1.05	2.1	0.28	41.5	0.38	0.8	0.42	58.5
	(2)		2.8				1.8		
Fe15Co5	(1)	1.06	2.1	0.25	39	0.37	0.8	0.40	61
	(2)	1.05	2.9			0.40	1.8		
Fe10Co10	(1)	1.06	2.1	0.24	32.5	0.36	0.8	0.40	67.5
	(2)	1.04	2.9			0.43	1.8		
Fe5Co15	(1)	1.09	2.1	0.21	25.5	0.37	0.8	0.39	74.5
	(2)	1.05	2.9			0.46	1.8		

[a] para, paramagnetic; δ, isomer shift (mm/s); ΔE_Q, quadrupole splitting (mm/s); Γ, line width (mm/s) of elemental doublet; P, proportion (%); (1) and (2) refer to the two components which are recognized in the respective probability-distribution profiles.

Since for the syntheses of the involved oxides stoichiometric mixtures of metal nitrates, aimed to eventually obtain $Mg_{0.8}(Fe/Co)_{0.2}Al_2O_4$ spinels, were used, the presence of Fe^{3+} implies that the obtained products are defective spinels, of which the general formula can be written as $(Mg_{1-x-y}^{2+}Fe_{x-3\alpha}^{2+}Fe_{2\alpha}^{3+}\square_\alpha Co_y^{2+}Al_2^{3+})O_4^{2-}$ in agreement with earlier results.[21]

Mössbauer Spectroscopy Study of CNT−Fe/Co−$MgAl_2O_4$ Nanocomposite Powders. The MS obtained at 80 K and at RT for Fe20R, Fe15Co5R, Fe10Co10R, and Fe5Co15R are reproduced in Figures 2 and 3, respectively. The corresponding Mössbauer parameters are listed in Tables 2 and 3, respectively. The results for Fe20R[17] are included for the sake of comparison. Because of being irrelevant, the weak Fe^{2+} doublet (P = 2%) detected for Fe20R at RT[17] is neglected in the present discussion.

Comparing the results for Fe20R and Fe15Co5R, it is noticed that the MS, both at 80 K (Figure 2a,b) and at RT (Figure 3a,b), exhibit similar global features, being composed of two sextets and one singlet. The narrower sextet ($H_{hf} \sim$ 250−240 kOe) and

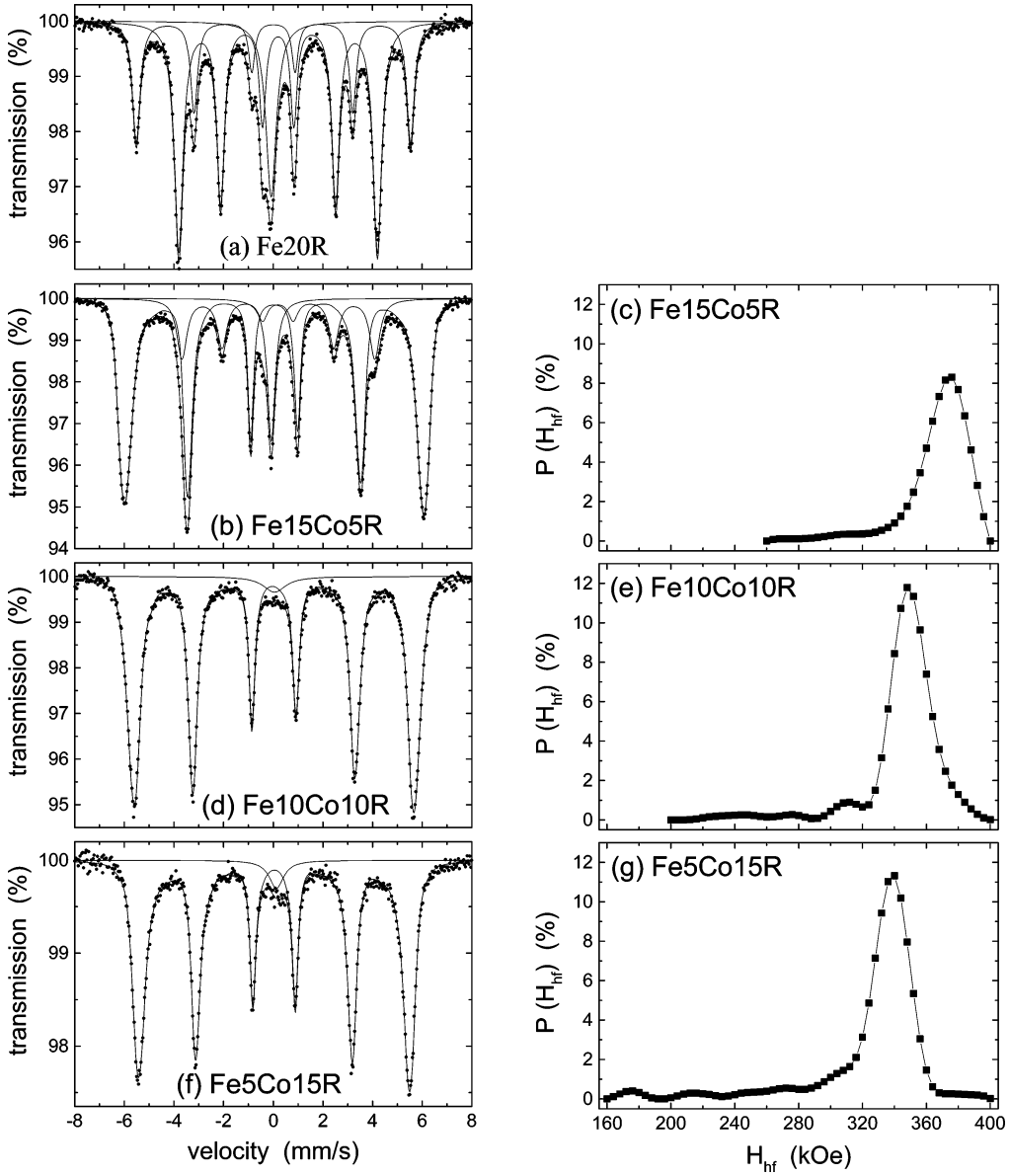

Figure 2. MS of Fe20R (a), Fe15Co5R (b), Fe10Co10R (d), and Fe5Co15R (f) measured at 80 K and corresponding hyperfine-field distributions of the ferromagnetic Fe/Co alloys (c, e, and g, respectively).

the singlet in the Fe15Co5R MS have Mössbauer parameters that are similar to those of the Fe_3C sextet and the γ-Fe−C singlet, respectively, resolved from the Fe20R spectra (Tables 2 and 3). Consequently, no Co atoms seem to be involved in these two phases. The Fe_3C proportion, however, is much lower in Fe15Co5R than in Fe20R. In contrast, the hyperfine fields H_{hf} for the dominant sextet components in the MS of Fe15Co5R are significantly higher than the corresponding values of the α-Fe sextet in Fe20R, the absorption lines for the former being also broader and slightly asymmetric (see Figures 2a,b and 3a,b). The broadened sextet components could only be adequately fitted using hyperfine-field distributions (HFDs) with linear correlations between isomer shift and hyperfine field and between quadrupole shift and hyperfine field. The field data indicated in Tables 2 and 3 refer to the maximum-probability values. The adjusted values of respective correlation coefficients, D_δ and D_ϵ, as well as the width Γ of the elemental sextet, are also included in these Tables. The hyperfine-field distributions at 80 K and at RT (Figures 2c and 3c) show a short tail toward low-field values. The quadrupole-shift values corresponding to maximum probability are consistently equal to zero, consistent with a cubic structure for the involved Fe-containing phase. The isomer-shift value at RT is slightly positive, and the hyperfine-field value is in excellent agreement with the value reported by Johnson et al.[27] for a body-centered cubic (bcc) α-$Fe_{0.75}Co_{0.25}$ alloy. It thus appears that the broad sextets present in the MS of Fe15Co5 are due to an Fe/Co alloy with an average composition close to the targeted one. The observed line broadening can then be ascribed to compositional fluctuations and/or small-particle-size effects.

Earlier Mössbauer spectroscopic measurements at various temperatures in the range 11 K to RT for the Fe/Co−$MgAl_2O_4$ nanocomposite powders obtained by reduction in pure H_2 at 1000 °C of $Mg_{0.9}Fe_{0.08}Co_{0.02}Al_2O_4$ and $Mg_{0.9}Fe_{0.065}Co_{0.035}Al_2O_4$ solid solutions[21] showed a unique sextet, with absorption lines broadened with respect to the line width observed for an α-Fe foil and with Mössbauer parameters that are in agreement with those found for the desired α-$Fe_{0.8}Co_{0.2}$ and α-$Fe_{0.65}Co_{0.35}$ alloys.[27] It appears that the presence of carbon in the presently applied reducing atmosphere favors the formation of Fe_3C and γ-Fe−C in the obtained iron-rich CNT−Fe/Co−$MgAl_2O_4$ nanocomposite powder. As a consequence, an amount of Co

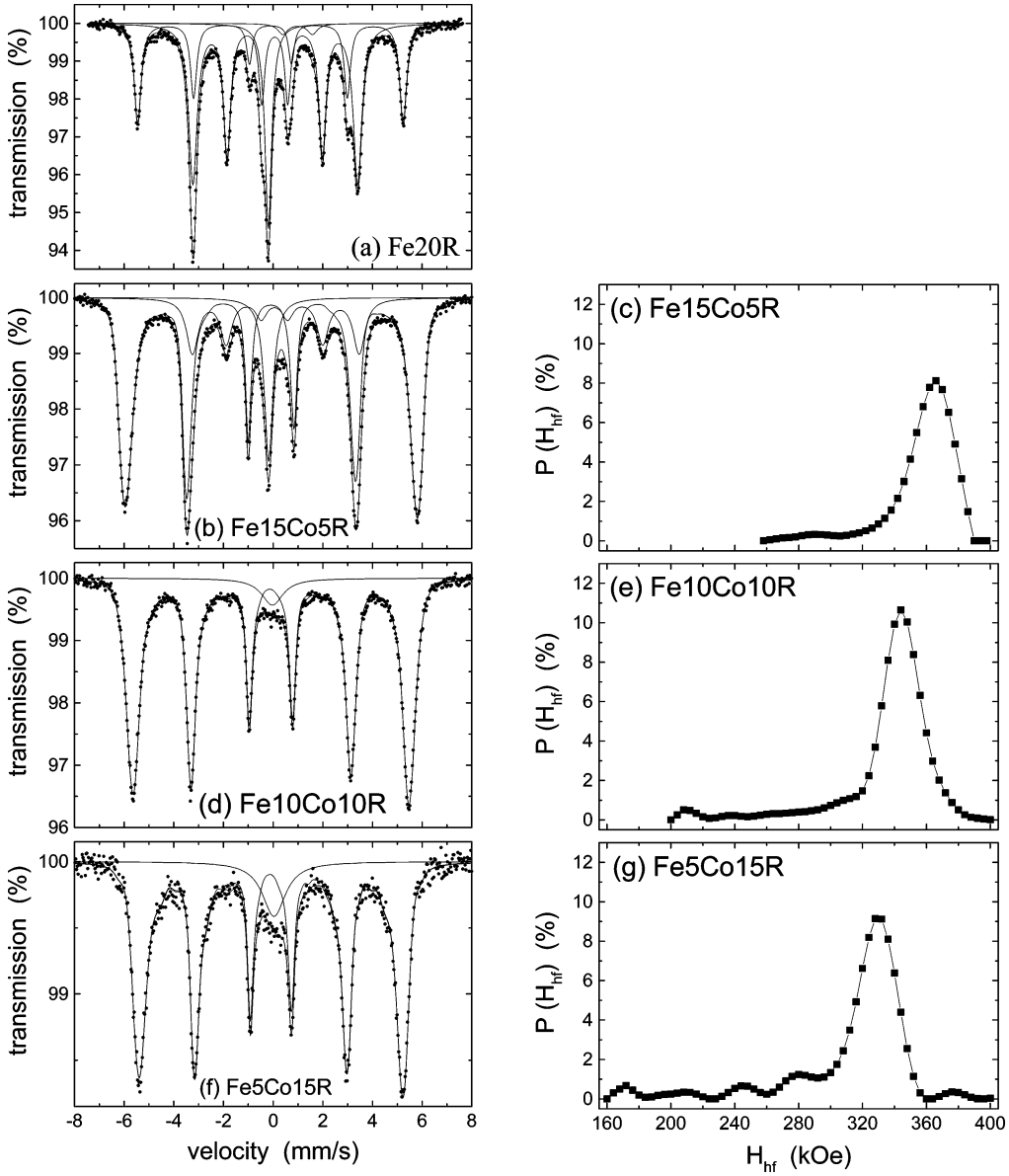

Figure 3. MS of Fe20R (a), Fe15Co5R (b), Fe10Co10R (d), and Fe5Co15R (f) measured at RT and corresponding hyperfine-field distributions of the ferromagnetic Fe/Co alloys (c, e, and g, respectively).

TABLE 2: Mössbauer Parameters of Fe20R, Fe15Co5R, Fe10Co10R, and Fe5Co15R Measured at 80 K[a]

composite powder	ferro Fe/Co (ferro α-Fe)							ferro Fe_3C					nonferro Fe (para γ-Fe−C)		
	δ	H_{hf}	$2\epsilon_Q$	D_δ	D_ϵ	Γ	P	δ	H_{hf}	$2\epsilon_Q$	Γ	P	δ	Γ	P
Fe20R	0.12	343	0[b]			0.29	27.5	0.31	248	0.00	0.32	59	0.03	0.51	13.5
Fe15Co5R	0.15	375[c]	0.00	0.0000	0.0014	0.25	72	0.30	240	0.02	0.45	19	0.03	0.38	9
Fe10Co10R	0.14	349[d]	0.01	0.0001	0.0014	0.27	97						0.16	1.10	3
Fe5Co15R	0.14	339[e]	0.00	0.0005	0.0010	0.25	96						0.23	0.70	4

[a] ferro, ferromagnetic; H_{hf}, hyperfine field at the maximum of the distribution (kOe); δ, isomer shift (mm/s); $2\epsilon_Q$, quadrupole shift (mm/s); D_δ, linear correlation coefficient between isomer shift and hyperfine field; D_ϵ, linear correlation coefficient between quadrupole shift and hyperfine field; Γ, Lorentzian line width (mm/s); P, proportion (%). [b] Fixed parameter [c] Hyperfine-field distribution from 260 to 400 kOe [d] Hyperfine-field distribution from 200 to 400 kOe [e] Hyperfine-field distribution from 160 to 400 kOe

atoms in excess to the amount required to form a uniform $Fe_{0.75}Co_{0.25}$ alloy composition with the still available Fe atoms, is present, resulting in compositional variations toward Co-richer Fe/Co alloys. Knowing that these alloys exhibit lower hyperfine fields.[27] as compared to $Fe_{0.75}Co_{0.25}$, the observed tail toward low-field values in the evaluated hyperfine-field distributions can be understood. The linear correlation coefficient D_δ between isomer shift and hyperfine field is negligible (see Tables 2 and 3) and hence the isomer shift can be considered constant for all hyperfine-field values considered in the distribution for Fe15Co5R, both at 80 K and at RT. In contrast, the quadrupole shift seems to increase with decreasing hyperfine field (positive linear correlation coefficients D_ϵ at 80 K and at RT), which could be indicative of increased deformations of the cubic structure for lower-field values, i.e., higher Co contents. However, this conclusion should be considered with necessary reserve.

TABLE 3: Mössbauer Parameters of Fe20R, Fe15Co5R, Fe10Co10R, and Fe5Co15R Measured at RT[a]

composite powder	ferro Fe/Co (ferro α-Fe)							ferro Fe_3C					nonferro Fe (para γ-Fe−C)		
	δ	H_{hf}	$2\epsilon_Q$	D_δ	D_ϵ	Γ	P	δ	H_{hf}	$2\epsilon_Q$	Γ	P	δ	Γ	P
Fe20R	0.00	332	0[b]			0.27	28	0.18	206	0.02	0.28	56	−0.08	0.33	14
Fe15Co5R	0.03	366[c]	0.00	0.0000	0.0016	0.26	70.5	0.19	210	0.06	0.54	19.5	−0.07	0.41	10
Fe10Co10R	0.02	344[d]	0.01	0.0001	0.0011	0.26	95						0.08	1.05	5
Fe5Co15R	0.02	330[e]	0.00	0.0004	0.0016	0.25	90						0.14	1.14	10

[a] ferro, ferromagnetic; H_{hf}, hyperfine field at the maximum of the distribution (kOe); δ, isomer shift (mm/s); $2\epsilon_Q$, quadrupole shift (mm/s); D_δ, linear correlation coefficient between isomer shift and hyperfine field; D_ϵ, linear correlation coefficient between quadrupole shift and hyperfine field; Γ, Lorentzian line width (mm/s); P, proportion (%). [b] Fixed parameter. [c] Hyperfine-field distribution from 260 to 400 kOe. [d] Hyperfine-field distribution from 200 to 400 kOe. [e] Hyperfine-field distribution from 160 to 400 kOe.

The MS of Fe10Co10R collected at 80 K and RT consist of a broad and slightly asymmetric sextet and a weak single line (Figures 2d and 3d). There is no indication whatsoever that a contribution from an Fe_3C phase or any other carbide phase is present. The isomer-shift value of the weak singulet is considerably higher than the value that is observed for the γ-Fe−C component appearing in the spectra of Fe15Co5R and Fe20R. Moreover, the former singlet is much broader and its fractional area is significantly higher at RT than at 80 K (Tables 2 and 3). The broad, asymmetric sextet components closely resemble those observed for the Fe15Co5R sample and as for the latter were quantified by HFDs. The as such obtained maximum-probability Mössbauer parameters at RT (Table 3) are in very good agreement with those found for α-$Fe_{0.50}Co_{0.50}$ alloy.[27]

The nature of the weak singlet component appearing in the MS of Fe10Co10R remains unclear. As mentioned above, its fractional area slightly decreases in favor of the sextet area when the temperature is lowered from RT to 80 K. The HFD profiles at 80 K and at RT show a longer tail toward low-field values for Fe10Co10R as compared to Fe15Co5R (Figures 2e and 3e) and the linear correlation coefficients between isomer shift and hyperfine field have a positive value (Tables 2 and 3). Considering the mathematical formulation of the theoretical line shape adjusted to the experimental data, a positive sign implies an increase of the isomer shift with decreasing hyperfine field toward values similar to those of the isomer shift of the singlet. Considering the mathematical formulation of the theoretical line shape adjusted to the experimental data, the positive correlation implies an increase of the isomer shift with decreasing hyperfine field and extrapolated to zero field the isomer shift reaches a value close to that of the isomer shift of the singlet. Together, these findings could indicate superparamagnetic behavior for the smallest particles in the distribution of the particle size of the Fe/Co alloy phase present in the Fe10Co10R powder. The superparamagnetic particles would then give rise to the singlet component in the MS, and consequently, being inherent to small-particle magnetic powders, the relative spectral area of the singulet decreases with decreasing temperature. However, this explanation for the presence of the weak central absorption has not a very sound basis, and at this point it cannot be excluded that a different phenomenon may be responsible.

In the case of Fe5Co15R, the HFDs at 80 K and at RT exhibit an even longer tail toward low-field values (Figures 2g and 3g) and the linear correlation coefficients between isomer shift and hyperfine field show higher values as compared to those of Fe10Co10R. The Mössbauer parameters at the maximum of the distribution at RT (Table 3) are in good agreement with the targeted α-$Fe_{0.25}Co_{0.75}$ alloy.[27] However, this composition corresponds to an alloy at the border of the transition region between the bcc α-Fe/Co structure and the face-centered cubic (fcc) γ-Fe/Co structure.[28] The isomer-shift values of the central absorption line as detected at 80 K and at RT are higher for Fe5Co15R than for Fe10Co10R. Also, its fractional areas are significantly higher, especially at RT. Hence, it appears that the single, central absorption line is promoted by a higher Co proportion, which could indicate that it might arise from a different type of alloy, e.g., with a γ-Fe/Co structure. These alloys have received far less attention than their α-counterparts. However, it is conceivable that the γ-Fe/Co fcc structure, with its large octahedral voids, would be favorable to the formation of a solid solution with carbon in interstitial positions. The γ-Fe/Co structure is the stable form at the applied reducing temperature (1070 °C).[28] In the presence of carbon, a γ-Fe/Co−C phase, which is most likely paramagnetic down to low temperatures, could be stabilized at RT, even for Co contents lower than the 90 atom % limit reported by Ellis and Greiner.[28] The increase of the isomer shift with increasing Co proportion could then be explained by the existence of compositional fluctuations. This phenomenon could be the explanation for the observed single absorption lines present in the MS of the Fe10Co10R and Fe5Co15R powders.

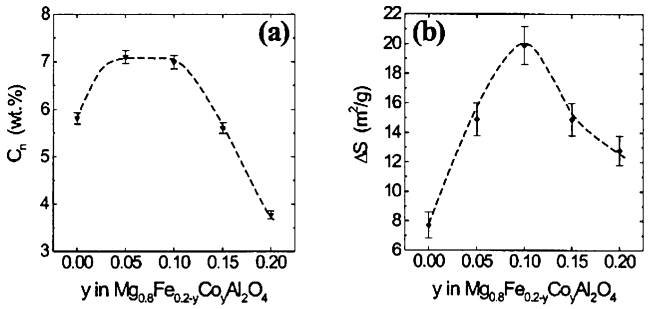

Figure 4. Carbon content C_n (a) and CNT quantity parameter ΔS (b) versus the Fe/Co alloy composition of the CNTs−Fe/Co−$MgAl_2O_4$ nanocomposite powders. The lines are guides to the eye.

It can thus be concluded that a very large proportion (70.5−95 atom %) of the Fe species in the CNT−Fe/Co−$MgAl_2O_4$ nanocomposite powders are α-Fe/Co alloys of the desired composition. The formation of Fe_3C is promoted for high Fe proportions, but no carbide is detected for equimolar Fe/Co proportions and higher Co proportions. For these compositions, a γ-Fe/Co−C phase, stable at RT, may be formed.

Relation between Fe Species and CNTs. As shown earlier,[5] the carbon content (C_n) in the CNT−Fe/Co−$MgAl_2O_4$ nanocomposite powders increases from Fe20R to reach a plateau for Fe15Co5R and Fe10Co10R and then decreases, the carbon content for Co20R being lower than that for Fe20R (Figure 4a). The CNTs quantity (ΔS) increases sharply between Fe20R and Fe10Co10R and then decreases for Fe15Co5R, its value for Co20R being about double that for Fe20R (Figure 4b).

The increase of the carbon content in the CNT−Fe/Co−$MgAl_2O_4$ nanocomposite powders was consequently correlated to the formation of CNTs. As mentioned above, studies of the

Fe−, Fe/Co−, and Co−$MgAl_2O_4$ powders[20,21] have revealed that the metal particle size distribution is bimodal (<30 nm and 50−200 nm) for Fe−$MgAl_2O_4$ but unimodal and rather narrow for Fe/Co− and Co−$MgAl_2O_4$ (10−15 nm). Hence, the evolution from Fe- to the Co-containing specimens probably reflects mainly the particle size difference, while the evolution between the various Co-containing powders probably indicates a better chemical activity of the Fe/Co alloys for the formation of CNTs as compared to pure Co, and with a maximum in that respect for the $Fe_{0.50}Co_{0.50}$ alloy, which exhibits optimal resistivity against deactivation that occurs through Fe_3C formation.

Conclusions

A detailed ^{57}Fe Mössbauer study of the $Mg_{0.8}Fe_{0.2-y}Co_yAl_2O_4$ ($y = 0$, 0.05, 0.1, 0.15, 0.2) solid solutions and of the CNT−Fe/Co−$MgAl_2O_4$ nanocomposite powders prepared by reduction in H_2-CH_4 has allowed characterization of the different iron phases involved in the catalytic process and correlation of these results with the microstructure of the powders (carbon content, CNTs content) reported earlier.[5] First, the study has shown that the oxide precursors consist of defective spinels of general formulas $(Mg_{1-x-y}^{2+}Fe_{x-3\alpha}^{2+}Fe_{2\alpha}^{3+}\square_\alpha Co_y^{2+}Al_2^{3+})O_4^{2-}$, similar to those of a different composition prepared earlier[21] by the same process. Second, the metallic phase in the CNT−Fe/Co−$MgAl_2O_4$ nanocomposite powders is mostly in the form of the ferromagnetic α-Fe/Co alloy with the desired composition. For high iron initial proportions, the additional formation of Fe_3C and γ-Fe−C is observed, while for high cobalt initial proportions, the additional formation of a γ-Fe/Co−C phase is favored. Iron appears to be chemically more active than cobalt for the decomposition of CH_4 at high temperature. However, the size distribution of the iron particles is difficult to control, resulting in a proportion of large particles that are inactive for CNT formation. Moreover, the formation of Fe_3C limits the catalytic activity, probably by early poisoning of the iron particles. The higher yield of CNTs is observed for postreaction α-$Fe_{0.50}Co_{0.50}$ catalytic particles, which form no carbide and have a narrow size distribution adequate for CNT formation. Alloying is beneficial for this system with respect to the formation of CNTs.

Acknowledgment. The authors thank Mr. L. Datas for his assistance in the TEM observations, which have been performed at the "Service Commun de Microscopie Electronique à Transmission, Université Paul-Sabatier". This research is supported by the Belgian National Program of Inter-University Attraction Pole on Reduced Dimensionality Systems (P4/10), by the Fund for Scientific Research−Flanders, and by the Franco−Belgian TOURNESOL program (T99/006-T99/045).

References and Notes

(1) Hafner, J. H.; Bronikowski, M. J.; Azamian, B. K.; Nikolaev, P.; Rinzler, A. G.; Colbert, D. T.; Smith, K. A.; Smalley, R. E. *Chem. Phys. Lett.* **1998**, *296*, 195.

(2) Flahaut, E.; Peigney, A.; Laurent, Ch.; Rousset, A. *J. Mater. Chem.* **2000**, *10*, 249.

(3) Bacsa, R. R.; Laurent, Ch.; Peigney, A.; Bacsa, W. S.; Vaugien, Th.; Rousset, A. *Chem. Phys. Lett.* **2000**, *323*, 566.

(4) Peigney, A.; Coquay, P.; Flahaut, E.; Vandenberghe, R. E.; De Grave, E.; Laurent, Ch. *J. Phys. Chem. B* **2001**, *105*, 9699.

(5) Flahaut, E.; Govindaraj, A.; Peigney, A.; Laurent, Ch.; Rousset, A.; Rao, C. N. R. *Chem. Phys. Lett.* **1999**, *300*, 236.

(6) Colomer, J.-F.; Bister, G.; Willems, I.; Konya, Z.; Fonseca, A.; Van Tendeloo, G.; Nagy, B. J. *Chem. Commun*. **1999**, 1343.

(7) Zhu, J.; Yudasaka, M.; Iijima, S. *Chem. Phys. Lett.* **2003**, *380*, 496.

(8) Chiashi, S.; Murakami, Y.; Miyauchi, Y.; Maruyama, S. *Chem. Phys. Lett*. **2004**, *386*, 89.

(9) Kukovecz, Z. N.; Konya, Z.; Nagaraju, I.; Willems, I.; Tamasi, A.; Fonseca, A.; Nagy, B. J.; Kiricsi, I. *Phys. Chem. Chem. Phys*. **2000**, *2*, 3071.

(10) Yang, Y.; Hua, Z.; Lu, Y. N.; Chen, Y. *Mater. Chem. Phys*. **2003**, *82*, 440.

(11) Pinheiro, J. P.; Gadelle, P. *J. Phys. Chem. Sol*. **2001**, *62*, 1015.

(12) Pinheiro, J. P.; Gadelle, P.; Jeandey, C.; Oddou, J. L. *J. Phys. Chem. Solids* **2001**, *62*, 1023.

(13) Avdeeva, L. B.; Reshetenko, T. V.; Ismagilov, Z. R..; Likholobov, V. A. *Appl. Catal., A* **2002**, *228*, 53.

(14) Reshetenko, T. V.; Avdeeva, L. B.; Khassin, A. A.; Kustova, G. M.; Ushakov, V. A.; Moroz, E. M.; Shmakov, A. N.; Kriventsov, V. V.; Kochubey, D. I.; Pavlyukhin, Yu. T.; Chuvilin, A. L.; Ismagilov, Z. R. *Appl. Catal., A* **2004**, *268*, 127.

(15) Reshetenko, T. V.; Avdeeva, L. B.; Ushakov, V. A.; Moroz, E. M.; Shmakov, A. N.; Kriventsov, V. V.; Kochubey, D. I.; Pavlyukhin, Yu. T.; Chuvilin, A. L.; Ismagilov, Z. R. *Appl. Catal., A* **2004**, *270*, 87.

(16) Konya, Z.; Kiss, J.; Oszko, A.; Siska, A.; Kiricsi, I. *Phys. Chem. Chem. Phys*. **2001**, *3*, 155.

(17) Coquay, P.; De Grave, E.; Vandenberghe, R. E.; Dauwe, C.; Flahaut, E.; Laurent, Ch.; Peigney, A.; Rousset, A. *Acta Mater*. **2000**, *48*, 3015.

(18) Peigney, A.; Laurent, Ch.; Dobigeon, F.; Rousset, A. *J. Mater. Res.* **1997**, *12*, 613.

(19) Govindaraj, A.; Flahaut, E.; Laurent, Ch.; Peigney, A.; Rousset, A.; Rao, C. N. R. *J. Mater. Res.* **1999**, *14*, 2567.

(20) Quénard, O.; Laurent, Ch.; Brieu, M.; Rousset, A. *Nanostruct. Mater*. **1996**, *7*, 497.

(21) Quénard, O.; De Grave, E.; Laurent, Ch.; Rousset, A. *J. Mater. Chem*. **1997**, *7*, 2457.

(22) Coquay, P.; Laurent, Ch.; Peigney, A.; Quénard, O.; De Grave, E.; Vandenberghe, R. E. *Hyp. Int.* **2000**, *130*, 275.

(23) Coquay, P.; De Grave, E.; Vandenberghe, R. E.; Peigney, A.; Laurent, Ch.. *Hyperfine Interact.* **2002**, *139−140*, 289.

(24) Peigney, A.; Laurent, Ch.; Flahaut, E.; Bacsa, R. R.; Rousset, A. *Carbon* **2001**, *39*, 507.

(25) Coquay, P.; Peigney, A.; De Grave, E.; Flahaut, E.; Vandenberghe, Laurent, Ch. *J. Phys. Chem. B* **2005**, *109*, 17813.

(26) Patil, K. C. *Bull. Mater. Sci*. **1993**, *16*, 533.

(27) Johnson, C. E.; Ridout, M. S.; Cranshaw, T. E. *Proc. Phys. Soc.* **1963**, *81*, 1079.

(28) Ellis, W. C.; Greiner, E. S. *Trans. Am. Soc. Met.* **1941**, *29*, 415.